

Simulation of Adsorption Process of L-Tryptophan on Mixed-Mode Resin HD-1 with Combined Physical Adsorption and Ion Exchange

Pengfei Jiao,* Xin Zhang, Yuping Wei, and Peng Wang

Cite This: *ACS Omega* 2022, 7, 35331–35338

Read Online

ACCESS |



Metrics & More

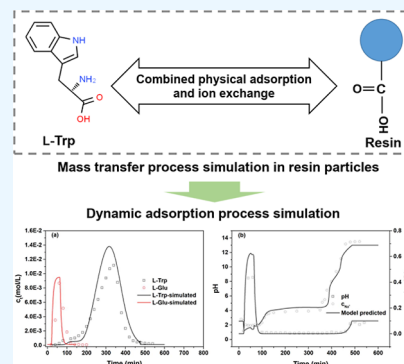


Article Recommendations



Supporting Information

ABSTRACT: The mass-transfer process of L-tryptophan (L-Trp) in the hydrophobic interaction/ion-exchange mixed-mode resin HD-1 particles and fixed bed was studied experimentally and theoretically. The adsorption kinetics of L-Trp in single-component and multicomponent adsorption systems was investigated under different pH conditions. The co-adsorption of sodium ions (Na^+) and L-Trp anions was found to be negligible. A modified liquid-film linear driving force model considering the physical adsorption of L-Trp zwitterions and anions as well as ion exchange of L-Trp cations was proposed. The dissociation equilibria of L-Trp molecules and functional groups on the resin were introduced in the model. The model could well fit the kinetic adsorption curves of L-Trp at different pH values. The presence of Na^+ and the impurity amino acid L-glutamic acid (L-Glu) did not significantly affect the mass-transfer rate of L-Trp. The dynamic adsorption processes of L-Trp under different pH and concentration conditions were studied. A modified transport-dispersive model considering axial diffusion, liquid-film mass transfer, and a combined physical adsorption and ion-exchange equilibrium was established, which could predict the adsorption breakthrough curves of L-Trp well. During the dynamic adsorption process, the pH of mobile phase in the fixed bed changed with changing the L-Trp concentration in the mobile phase. L-Trp was well separated from Na^+ and L-Glu with the purity of L-Trp higher than 99%, the recovery rate higher than 95%, and a concentration of 4.69×10^{-3} mol/L. The elution chromatographic peaks of L-Trp, L-Glu, and Na^+ and the pH of the outlet solution were predicted satisfactorily.



1. INTRODUCTION

Mixed-mode chromatography is a new chromatographic separation technique. The adsorbents used in the separation technique contain specially designed ligands, which can interact with adsorbates via two or more interaction forces, including hydrogen bond, hydrophobic interaction, electrostatic force, and so forth.^{1–3} Compared with the traditional single-mode chromatographic separation techniques, including ion-exchange chromatography, hydrophobic interaction chromatography, and hydrophilic interaction chromatography, mixed-mode chromatography has significant advantages such as high adsorption capacity, strong salt tolerance, mild elution, and regeneration conditions.^{4–6} Therefore, the technique has been widely used in the preparative separation of many biochemical products, including amino acids, nucleosides, peptides, and so on.^{7–9}

The mathematical modeling of the mass-transfer process of preparative chromatography plays an important role in the design and optimization of an efficient separation process.¹⁰ Especially for the mixed-mode chromatographic separation process, the complexity of functional groups on the adsorbents increases the controllable factors of the operation process but also increases the difficulty of optimizing the operating conditions of the separation process. It is necessary to construct accurate mathematical models for mixed-mode chromatography. At present, the mathematical modeling of

mixed-mode chromatography has been studied by many researchers.^{11–16} Chester proposed a partition model with a new method for calculating the retention factor, which was applicable to predict the retention time of adsorbates in mixed-mode chromatographic separation process.¹⁶ Gomes et al. developed an expanded bed adsorption model taking into account the particle size distribution and bed voidage axial variation. The model predicted the albumin and immunoglobulin G adsorption breakthrough curves in an expanded bed column packed with a new mixed-mode adsorbent MabDirect MM satisfactorily.¹⁵ In our previous work, the mass-transfer process model considering the dissociation equilibrium of nucleotides and resin was established.¹⁷ The model provided a prediction to the dynamic adsorption and separation process of guanosine 5'-monophosphate and cytidine 5'-monophosphate by mixed-mode resin HD-1 satisfactorily.¹⁷ The nucleotides were adsorbed by the resin via physical adsorption. However, the mass-transfer process model considering the physical

Received: August 12, 2022

Accepted: September 19, 2022

Published: September 25, 2022



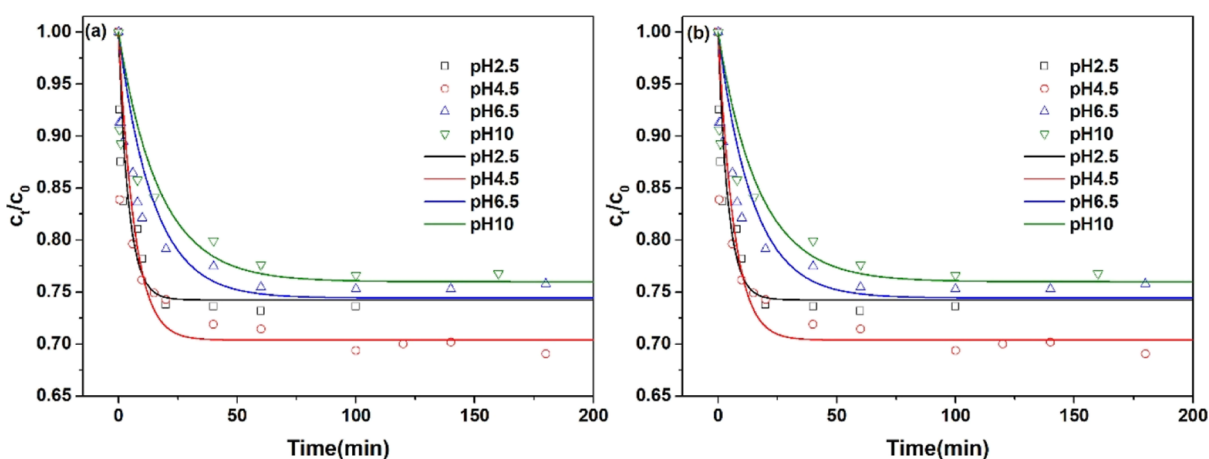


Figure 1. Kinetic adsorption curves measured experimentally and predicted by the model: (a) considering co-adsorption and (b) without considering co-adsorption.

Table 1. Adsorption Kinetic Model Parameters for L-Trp

	run 1	run 2	run 3	run 4
pH	2.5	4.5	6.5	10
k_{eff} (cm/min)	9.54×10^{-3}	6.51×10^{-3}	6.17×10^{-3}	4.77×10^{-3}
ARD %	5.61	6.17	6.85	5.82

adsorption and ion exchange of adsorbates as well as the dissociation equilibrium of adsorbates and adsorbents has never been reported.

L-Trp is one of the essential amino acids in human and animal bodies.¹⁸ It has been widely used in food, medicine, agriculture, and other fields.^{19–21} At present, the most commonly used method for L-Trp preparation is micro-organism fermentation.^{22,23} After pretreatment to remove microbial cells, proteins, pigments, and other impurities, the fermentation broth of L-Trp contains not only soluble salts (represented by NaCl) but also L-Glu, a major amino acid impurity.²⁴ The separation and purification of L-Trp is one of the key steps to restrict its efficient production. The most commonly used method for L-Trp separation is ion exchange.^{25,26} However, the high concentration of salts in the fermentation broth could reduce the ion-exchange capacity and separation efficiency of ion exchangers. Moreover, a lot of strong acids and bases need to be consumed to regenerate the ion exchangers. In our previous work, the weakly polar hyper-cross-linked adsorption resin XDA-200 was used to separate L-Trp mainly depending on the hydrophobic interaction.²⁷ This method could avoid the influence of soluble salt and L-Glu. However, the elution of L-Trp was difficult because of the strong hydrophobic interaction between the resin and indoles in L-Trp molecules. Thus, the chromatographic peak tailing for L-Trp was serious. The concentration of L-Trp in the products was not high enough. The hydrophobic interaction/ion-exchange mixed-mode adsorbent HD-1 was used to separate L-Trp in our research group.²⁸ The adsorbent could adsorb L-Trp mainly by hydrophobic interaction and ion exchange, and efficient elution was achieved by the electrostatic repulsive force. The unfavorable influence of L-Glu and soluble salts on L-Trp adsorption was avoided. The tail of the chromatographic peak was improved. The adsorption equilibrium behavior of L-Trp on the resin was studied in detail. It was found that different forms of L-Trp could be adsorbed by the resin. The adsorption equilibrium model combining physical adsorption

and ion exchange was constructed, which fitted the adsorption isotherms of L-Trp at different pH values. However, the mass-transfer process simulation of L-Trp in the resin particles and fixed bed needs to be further studied.

Based on our previous work, the simulation of mass-transfer process of L-Trp in the mixed-mode adsorbent HD-1 with combined physical adsorption and ion exchange as well as dissociation equilibrium of L-Trp and resin was studied. First, the adsorption kinetics of L-Trp in single-component and multicomponent adsorption systems was investigated, and the mass-transfer process model with adsorption of L-Trp at different forms was constructed. Second, the dynamic adsorption process of L-Trp was studied, and the column dynamic separation process model was constructed to simulate the breakthrough curves of L-Trp under different pH and concentration conditions. The pH and L-Trp concentration distribution in the column was analyzed. Finally, the dynamic separation process of L-Trp, L-Glu, and NaCl was simulated. The work carried out in this paper is valuable for the accurate simulation of mixed-mode chromatographic separation process and has reference significance for optimizing the separation process of L-Trp analogues.

2. RESULTS AND DISCUSSION

2.1. Mass-Transfer Process of L-Trp in Resin Particles.

The kinetic adsorption curves of L-Trp in the single-component adsorption systems are shown in Figure 1. The Na⁺ in the solution may adsorb on the resin by electrostatic attraction between L-Trp anions and Na⁺.²⁴ In order to investigate whether the co-adsorption of Na⁺ and L-Trp anions is negligible, the modified liquid-film linear driving force models with and without Na⁺ co-adsorption were used to fit the adsorption kinetics data of L-Trp at different pH values. The fitting curves are shown in Figure 1a and 1b, respectively. It can be seen from the figure that there is no significant difference in the fitting results of the two models. The results indicate that the co-adsorption of Na⁺ and L-Trp⁻ can be

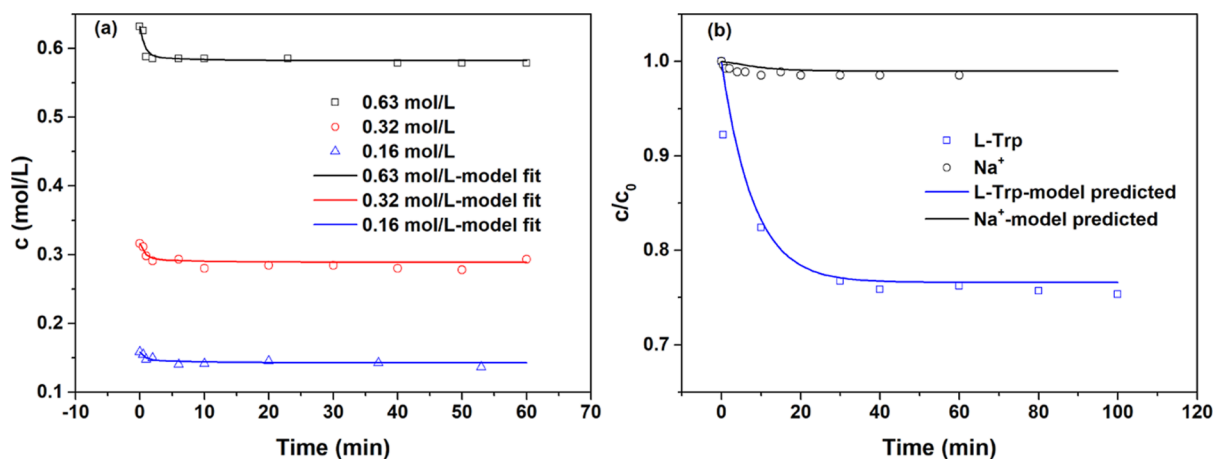


Figure 2. (a) Kinetic adsorption curves of Na^+ in a single-component adsorption system and (b) kinetic adsorption curves of L-Trp and Na^+ in a three-component adsorption system.

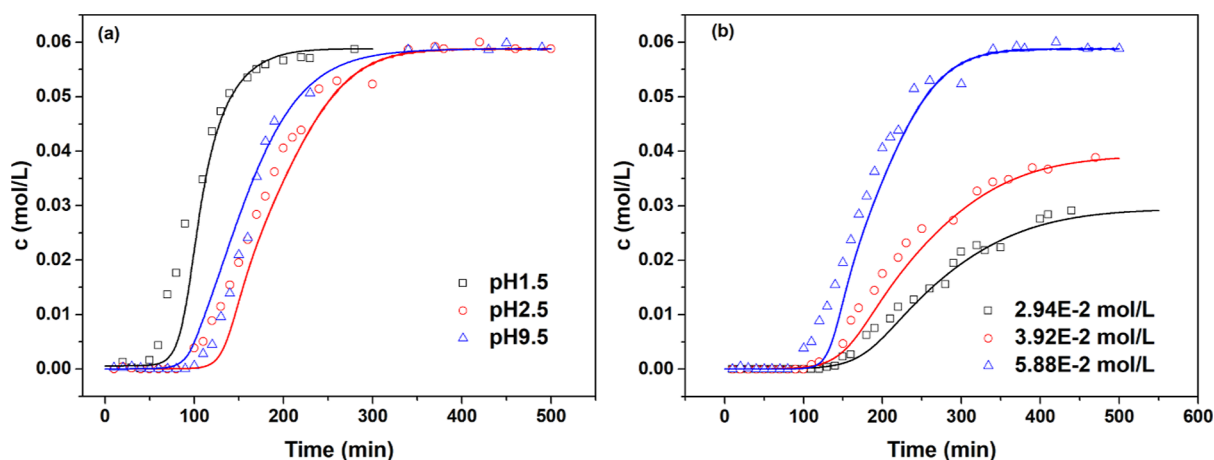


Figure 3. Adsorption breakthrough curves of L-Trp: (a) at different pH values and (b) at different concentrations. The solid lines are the curves predicted by the model.

neglected. It is due to that the reduction in Na^+ concentration in the liquid solution by co-adsorption with L-Trp^- is insignificant compared to the reduction in Na^+ concentration due to ion exchange of Na^+ with H^+ on the resin. Therefore, in the subsequent experiments, the adsorption kinetic model without considering the co-adsorption of Na^+ was adopted. The model parameters obtained by fitting the adsorption kinetics data of L-Trp to this model are shown in Table 1. It can be seen from Table 1 that the values of ARD % under different pH conditions are all lower than 7.0, indicating that the model considering the physical adsorption of L-Trp zwitterions and anions as well as ion exchange of L-Trp cations can well fit the kinetic adsorption curves. The values of effective diffusivity at pH 6.5 and 10 are lower than those at pH 2.5 and 4.5, indicating that the mass-transfer rate of L-Trp molecules at pH 6.5 and 10 is slower. The reason may be that the electrostatic repulsive force between L-Trp molecules and the resin at pH 6.5 and 10 prevents the diffusion of L-Trp molecules in the adsorbent particles to a certain extent. Kekenés-Huskey et al. found the identical phenomenon that the electrostatic repulsive force can depress the effective diffusion rates of ions.²⁹

The kinetic adsorption curves of Na^+ on HD-1 resin under different initial concentrations are shown in Figure 2a. The modified liquid-film linear driving force model was used to fit

the adsorption kinetics data, and the fitted curves are also shown in Figure 2a. It can be seen from the figure that the model can fit the adsorption kinetics data well.

The kinetic adsorption curves of L-Trp in a three-component adsorption system are shown in Figure 2b. The modified liquid-film linear driving force model was used to predict the adsorption kinetics data. It is found that there is no significant deviation between the predicted and experimental results, indicating that the model can well predict the adsorption kinetics data of the three-component adsorption system. L-Glu hardly adsorbed on HD-1 resin. Therefore, the concentration of L-Glu hardly changes. The kinetic adsorption curve of L-Glu is not shown in this work. In summary, the mass-transfer process of L-Trp on the resin in single- and three-component adsorption systems can be well simulated by the adsorption kinetic model proposed in this paper.

2.2. Mass-Transfer Process of L-Trp in a Fixed Bed Packed with HD-1 Resin. The adsorption breakthrough curves of L-Trp under different pH conditions are shown in Figure 3a. As can be seen from the figure, when pH is ~ 1.5 , the stoichiometric time of L-Trp (the concentration at the outlet of the fixed bed reaches 0.5 of the concentration of the feed solution) is the shortest. The stoichiometric time is the longest when pH is ~ 2.5 . The adsorption capacity at pH 1.5 is lower than that at pH 9.5 and 2.5, so the time needed for L-Trp to

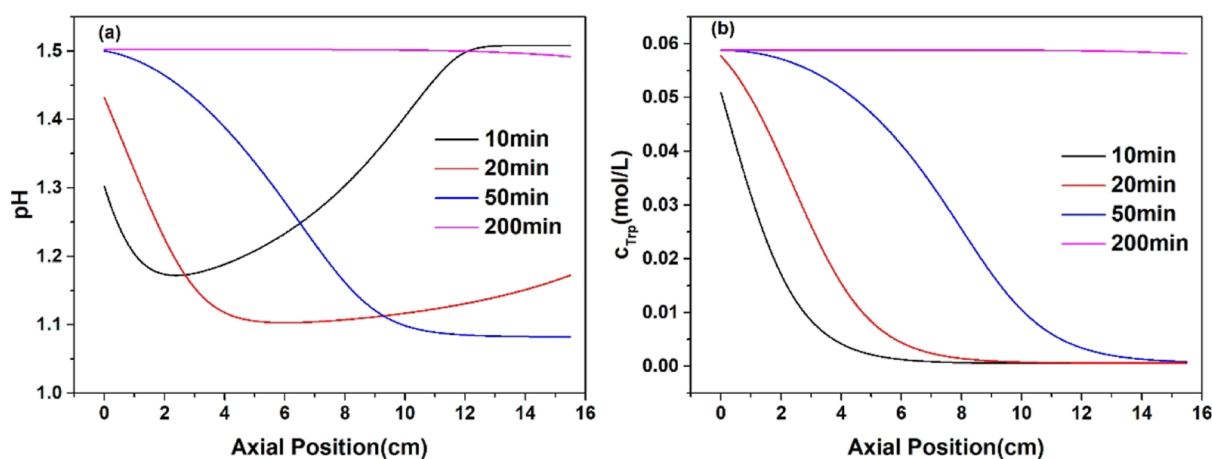


Figure 4. (a) Axial pH distribution and (b) axial concentration distribution of L-Trp in the mobile phase during adsorption when the pH of the feed solution is ~ 1.5 .

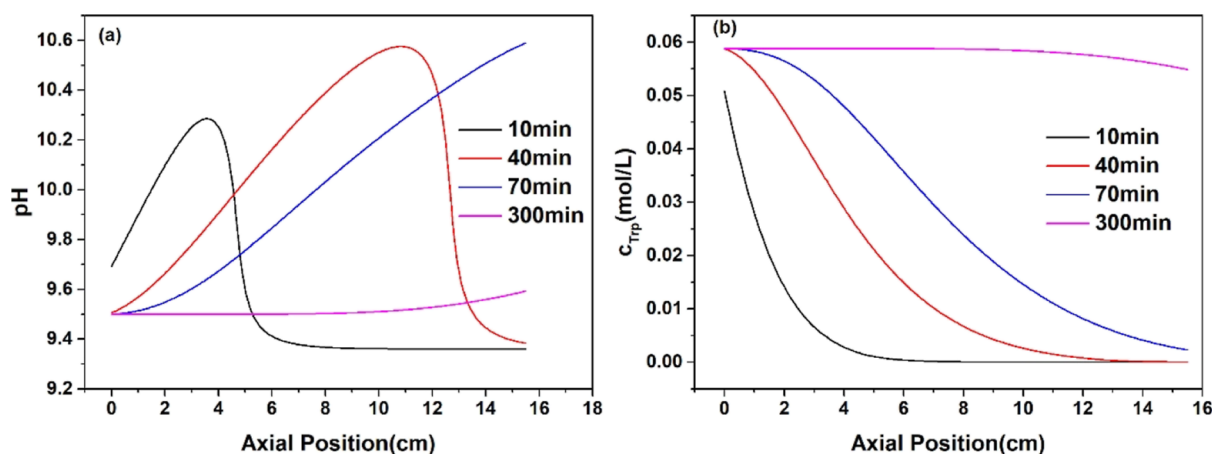


Figure 5. (a) Axial pH distribution and (b) axial concentration distribution of L-Trp in the mobile phase during adsorption when the pH of the feed solution is ~ 9.5 .

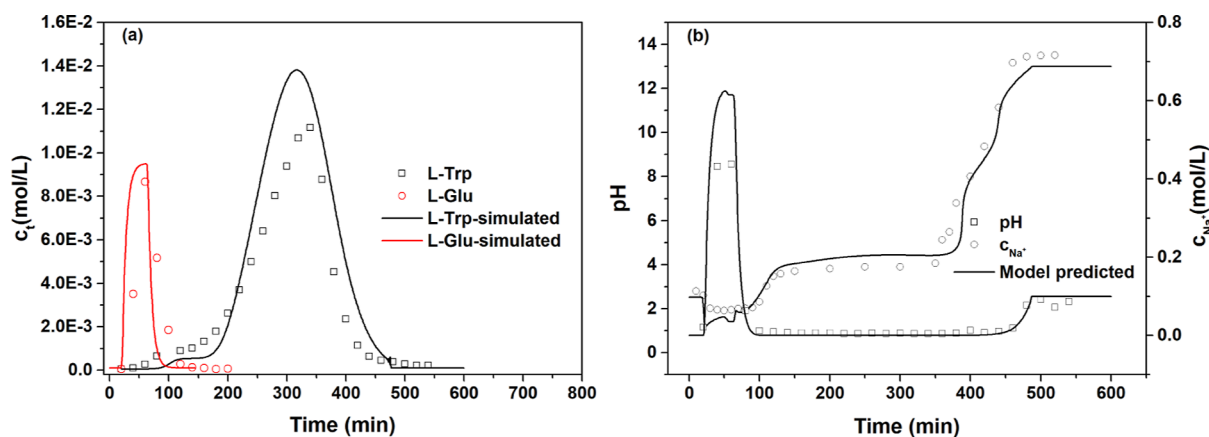


Figure 6. (a) Chromatographic peaks of L-Trp and L-Glu and (b) pH and concentration of Na⁺ at the outlet of the column.

reach adsorption saturation is the shortest at pH 1.5. The adsorption breakthrough curves of L-Trp at different feed concentrations are shown in Figure 3b. As can be seen from the figure, the stoichiometric time of L-Trp decreases with increasing concentration of the feedstock. For convex adsorption isotherms, the retention time of the adsorbent becomes shorter with increasing solution concentration.³⁰ The pH of the feed solution is ~ 2.5 . At pH 2.5, the L-Trp

adsorption isotherm is convex.²⁸ Therefore, the above results are reasonable.

The modified transport-dispersive model was used to fit the adsorption breakthrough curves of L-Trp, and the fitted curves are shown in Figure 3 as well. As can be seen from the figure, the model can provide a general prediction to the adsorption breakthrough curves. The concentration of L-Trp and pH in the mobile phase in the fixed bed varies with the axial position.

The concentration distribution of L-Trp and pH distribution in the mobile phase in the fixed bed were analyzed when the pH of the feed solution was ~ 1.5 and 9.5 . The results predicted by the model are shown in Figures 4 and 5. It can be seen from Figure 4b that the concentration of L-Trp in the mobile phase in the fixed bed increases gradually from the inlet to the outlet with the extension of adsorption time. From the comparison of Figure 4a,b, it can be seen that the pH of the mobile phase at the concentration front of L-Trp is lower than that at the other sites. The reason may be that some L-Trp cations exchange with hydrogen ions on the resin. The hydrogen ions are released into the mobile phase, resulting in a decrease in pH. By comparing Figure 5a,b, it is found that the pH of the mobile phase at the concentration front of L-Trp is higher than that at the other sites. The reason may be that the concentration of L-Trp in the mobile phase at the concentration front of L-Trp decreases, while the concentration of Na^+ hardly changes. Therefore, the concentration of H^+ decreases due to the need for electrical neutrality, leading to an increase in the pH of mobile phase.

2.3. Dynamic Separation Process of L-Trp, L-Glu, and NaCl. The experimental and predicted chromatographic peaks of L-Trp and L-Glu at the exit of the fixed bed are shown in Figure 6a. L-Trp was well separated from Na^+ and L-Glu with the purity of L-Trp higher than 99%, the recovery rate higher than 95%, and a concentration of 4.69×10^{-3} mol/L. The values of model parameters are listed in Table 2. As can be

Table 2. Operating and Model Parameters for the Dynamic Separation Process

parameter	value
bed height (cm)	15.5
$D_{\text{ax,Trp}}$ (cm^2/min)	9.79×10^{-3}
$D_{\text{ax,Glu}}$ (cm^2/min)	9.83×10^{-3}
$D_{\text{ax,Na}}$ (cm^2/min)	9.94×10^{-3}
$D_{\text{ax,Cl}}$ (cm^2/min)	1.04×10^{-2}
$k_{\text{eff,Trp}}$ (cm/min)	6.75×10^{-3}
$k_{\text{eff,Na}}$ (cm/min)	9.50×10^{-3}

seen from Figure 6a, the model can provide a general prediction to the chromatographic peaks. The deviation between the predicted and experimental results may result from the deviation between the calculated axial diffusion or mass-transfer parameters and the actual values of the parameters. The changing curves of solution pH and Na^+ concentration at the column outlet are shown in Figure 6b. The NaOH aqueous solution at a concentration of 0.1 mol/L was used as an eluent. The concentration of Na^+ increased to 0.1 mol/L slowly until eluting for more than 400 min. The result is due to that Na^+ is exchanged by H^+ on the resin. When eluting for about 20 min, the pH at the outlet of the column began to decrease. The result is due to that H^+ on the resin exchanged with Na^+ and L-Trp⁺ in the feed solution and flowed into the mobile phase. Therefore, the pH decreased. When eluting for about 400 min, the pH increased quickly to about 13. At this moment, H^+ on the resin was almost exchanged by Na^+ completely. As can be seen from Figure 6b, the model can provide a general prediction to the changing trend of pH and Na^+ . In sum, the model proposed in this paper can be used to simulate the mass-transfer process of L-Trp and optimize the L-Trp separation process.

3. CONCLUSIONS

The mass-transfer process of L-Trp in mixed-mode resin HD-1 particles and fixed bed was studied. The co-adsorption between Na^+ and L-Trp anions on the resin is negligible. The modified liquid-film linear driving force model considering the adsorption equilibrium behavior of L-Trp in different dissociation states as well as the dissociation equilibrium of L-Trp and functional groups of resin was proposed. The model can well fit the kinetic adsorption curves of L-Trp at different pH values. The model also predicted the concentration decay curves of L-Trp and Na^+ in the three-component adsorption system satisfactorily. In the fixed bed, L-Trp was well separated from Na^+ and L-Glu with the purity of L-Trp higher than 99%, the recovery rate higher than 95%, and a concentration of 4.69×10^{-3} mol/L. The modified transport-dispersive model considering the axial diffusion, liquid-film diffusion, and a combined physical adsorption and ion-exchange equilibrium constructed in this paper can well predict the adsorption breakthrough curves of L-Trp and the elution chromatographic peaks of the three-component adsorption system as well as the pH history. The mass-transfer process of L-Trp in resin particles and fixed bed can be well simulated by the models proposed in this paper. The research carried out in this paper has certain reference significance for optimizing the separation process of L-Trp analogues and can provide for accurate simulation of the mixed-mode chromatographic separation process.

4. MATERIALS AND METHODS

4.1. Resin. The functional group of resin HD-1 is the carboxyl group, and the backbone is polystyrene-divinylbenzene. The physicochemical properties of the resin were described in our previous work.²⁸

4.2. Chemicals. L-Trp, L-Glu, NaCl, sodium acetate, $\text{KH}_2\text{PO}_4 \cdot 3\text{H}_2\text{O}$, acetic acid, 2,4-dinitrofluorobenzene, and NaHCO_3 were purchased from Shanghai Macklin Biochemical Technology Co., Ltd. (Shanghai, China). NaOH was provided by Tianjin Jinbei Fine Chemical Co., Ltd. (Tianjin, China). Hydrochloric acid was purchased from China Pingmei Shenma Group Kaifeng Dongda Chemical Co., Ltd. All the above reagents were analytically pure. Acetonitrile (chromatographic pure reagent) was purchased from Tianjin Kemiou Chemical Reagent Co., Ltd. (Tianjin, China).

4.3. Determination of Kinetic Adsorption Curves of L-Trp. An aqueous solution of L-Trp (250 mL) was placed in a 500 mL round-bottomed flask. The pH of the solution was adjusted to ~ 2.5 with hydrochloric acid. The initial concentration of L-Trp was $\sim 3.18 \times 10^{-2}$ mol/L. The wet resin HD-1 (10 g) was added to the flask and mechanically stirred. Several samples were taken at preset time points (0.5, 1, 2, 6, 10, 20, 40, 60, and 100 min), and the concentration of L-Trp was measured by an ultraviolet–visible spectrophotometer after a certain dilution. The change curve of L-Trp concentration with time is the kinetic adsorption curve at pH 2.5.

The kinetic adsorption curves at other initial pH values were determined using identical operating steps as mentioned above. The kinetic adsorption curves of sodium chloride at different initial concentrations and that of the three-component mixture (L-Trp, L-Glu, and NaCl) were determined by the same method as mentioned above. The concentrations

of L-Trp, L-Glu, and NaCl in the three-component mixture were 5.88×10^{-2} , 9.52×10^{-3} , and 0.63 mol/L , respectively.

4.4. Determination of Adsorption Breakthrough Curves of L-Trp. An aqueous solution of L-Trp ($\sim 5.88 \times 10^{-2} \text{ mol/L}$) was passed from the upper end into a glass column (inner diameter 1.15 cm) filled with 10 g of HD-1 resin. The pH of the solution was ~ 2.5 . The flow rate at the column outlet was kept at $\sim 0.4 \text{ mL/min}$ by a peristaltic pump (BT100-1 L, Hebei, China). A collector (BSZ-100, Shanghai, China) was used to collect the effluent at the exit of the column at preset time points, and the concentration of L-Trp was measured after dilution. Until the concentration of L-Trp was close to that of the raw liquid, the injection was stopped. The changing curve of L-Trp concentration with time is the breakthrough curve at pH 2.5. The adsorption breakthrough curves at other pH values and different concentrations of feed solution were determined by the same procedures as mentioned above.

4.5. Determination of Chromatographic Elution Peak for L-Trp. About 13 mL of aqueous mixture of L-Trp, L-Glu, and NaCl ($\sim 5.88 \times 10^{-2}$, 9.52×10^{-3} , and 0.63 mol/L , respectively) was passed into a glass column (inner diameter 1.15 cm) filled with HD-1 resin (10 g). Then, the column was eluted with NaOH aqueous solution (0.1 mol/L) until the concentration of L-Trp at the column outlet approached 0. The flow rate was $\sim 0.3 \text{ mL/min}$. Other procedures and operating conditions are the same as that in Section 4.4. The change curves of L-Trp, L-Glu, and Na^+ concentration at the column exit with time are the chromatographic elution peaks.

The experiments in this paper were repeated three or more times. The data shown here is the average of three data sets. The experimental error was less than 6.0%.

4.6. Analytical Methods. The concentration of L-Trp was measured by a UV-visible spectrophotometer (BioSpectrometer, Eppendorf AG) with a wavelength of 218 nm. The concentration of L-Glu was determined by HPLC (LC-20AT, Shimadzu Corporation), and the determination method was the same as that in ref 27. The concentration of Na^+ was determined using a Na^+ concentration meter (DWS-295F, Shanghai Instrument Electric Science Instrument Limited by Share Ltd.). The solution pH was measured using a pH meter (FE28, Mettler Toledo International Co., Ltd).

5. THEORY

5.1. Modified Liquid-Film Linear Driving Force Model. The total mass conservation equation for the adsorption system is as follows

$$V \frac{dc_{b,i}}{dt} + m \frac{dq_i}{dt} = 0 \quad (1)$$

where V is the volume of the solution (mL), m is the mass of the resin (g), t is the time (min), $c_{b,i}$ is the concentration of the solute i in the liquid phase (mol/L), and q_i is the adsorption capacity (mmol/g).

The mass conservation equation in the particle phase is as follows

$$\varepsilon_p \frac{dc_{p,i}}{dt} + \rho \frac{dq_i}{dt} = k_{\text{eff},i} \frac{3}{R} (c_{b,i} - c_{p,i}) \quad (2)$$

where ε_p is the resin porosity, $c_{p,i}$ is the solute concentration in the resin pores (mol/L), ρ is the wet apparent density of the

resin (g/mL), $k_{\text{eff},i}$ is the effective diffusivity (cm/min), R is the resin particle diameter (cm).

The electroneutral relationship in the liquid phase in the resin pores is as follows

$$c_{p,\text{H}^+} + c_{p,\text{Trp}^+} + c_{p,\text{Na}^+} + c_{p,\text{Glu}^+} = c_{p,\text{Trp}^-} + c_{p,\text{Glu}^-} + c_{p,\text{Glu}^{2-}} + c_{p,\text{OH}^-} + c_{p,\text{Cl}^-} \quad (3)$$

where c_{p,H^+} , c_{p,Trp^+} , c_{p,Na^+} , c_{p,Glu^+} , c_{p,Trp^-} , c_{p,Glu^-} , $c_{p,\text{Glu}^{2-}}$, c_{p,OH^-} , and c_{p,Cl^-} are the concentrations of H^+ , L-Trp⁺, Na^+ , L-Glu⁺, L-Trp⁻, Glu⁻, Glu²⁻, OH⁻, and Cl⁻, respectively, in the resin particle pores (mol/L).

The dissociation process of L-Trp and L-Glu molecules as well as the calculation method of the concentration of L-Trp and L-Glu at different forms can be found in our previous work.²⁴

The relationship between H^+ concentration, OH⁻ concentration, and pH in the liquid phase in resin particle pores can be expressed by the following formulas

$$c_{p,\text{H}^+} \times c_{p,\text{OH}^-} = 10^{-14} \quad (4)$$

$$c_{p,\text{H}^+} = 10^{-\text{pH}} \quad (5)$$

The adsorption equilibrium relationship of L-Trp between the solid and liquid phases can be found in our previous work.²⁸ In this work, the adsorption isotherms at different pH values and the adsorption equilibrium model equations are shown simply in the Supporting Information. L-Glu molecules almost do not adsorb on the resin, so the adsorption amount of L-Glu is considered to be 0.

Considering the co-adsorption of Na^+ and L-Trp anions, the adsorption equilibrium relationship of Na^+ can be expressed by the following equation

$$q_{\text{Na}^+} = \frac{1.24\alpha S_{\text{Na-H}} c_{p,\text{Na}^+}}{c_{p,\text{H}^+} + S_{\text{Na-H}} c_{p,\text{Na}^+}} + q_{\text{Trp}^-} \quad (6)$$

where α is the dissociation degree of the resin. $S_{\text{Na-H}}$ is the ion-exchange selectivity coefficient between Na^+ and H^+ on the resin. The value of $S_{\text{Na-H}}$ is 0.015.¹⁷

The initial conditions of the adsorption system are as follows

$$c_{b,i} = c_{\text{fe},i} \quad (7)$$

$$q_i = 0 \quad (8)$$

The above model equations were solved by MATLAB 2010a. The partial differential equations were discretized into ordinary differential equations by a central difference method. Then, ODE23 was used to solve the ordinary differential equations. The relative and absolute tolerance is 10^{-5} .

The value of k_{eff} is obtained by minimizing the following objective function.

$$\text{Minimum} = \sum_{j=1}^N \left(\frac{c_{j,\text{exp}} - c_{j,\text{pred}}}{c_{j,\text{exp}}} \right)^2 \quad (9)$$

where $c_{j,\text{exp}}$ and $c_{j,\text{pred}}$ are the solute concentrations measured experimentally and calculated by the model, respectively. N is the number of experimental data points.

The average relative deviation (ARD %) between the experimental data for adsorption kinetics and the data calculated by the model can be expressed by the following equation

$$\text{ARD \%} = \frac{1}{N} \sum_{j=1}^N \left| \frac{c_{j,\text{exp}} - c_{j,\text{pred}}}{c_{j,\text{exp}}} \right| \times 100 \quad (10)$$

5.2. Modified Transport-Dispersive Model. The axial mass conservation equation of L-Trp and Na⁺ in the mobile phase inside the column is as follows

$$\frac{\partial c_i}{\partial t} + \frac{1 - \varepsilon_b}{\varepsilon_b} \frac{\partial(\varepsilon_p c_{p,i} + \rho q_i)}{\partial t} + v \frac{\partial c_i}{\partial z} = D_{\text{ax},i} \frac{\partial^2 c_i}{\partial z^2} \quad (11)$$

where ε_b is the void fraction of the fixed bed. v is the interstitial velocity (cm/min). z is the axial position in the fixed bed (cm). $D_{\text{ax},i}$ is the axial diffusion coefficient (cm²/min).

The axial mass conservation equation of Cl⁻ in the mobile phase in the column is as follows

$$\frac{\partial c_i}{\partial t} + v \frac{\partial c_i}{\partial z} = D_{\text{ax},i} \frac{\partial^2 c_i}{\partial z^2} \quad (12)$$

The mass conservation equation in the particle phase is expressed by eq 2.

The adsorption equilibrium relationship for L-Trp between the solid and liquid phases can be found in our previous work.²⁸ The adsorption equilibrium relationship for Na⁺ between the solid and liquid phases is expressed by eq 6.

The boundary conditions at the inlet and outlet of the fixed bed and the initial conditions of the system are as follows

$$z = 0(\text{inlet}) \quad D_{\text{ax},i} \frac{\partial c_i}{\partial z} = v(c_i|_{z=0} - c_{\text{in},i}) \quad (13)$$

$$z = L(\text{outlet}) \quad \frac{\partial c_i}{\partial z} \Big|_{z=L} = 0 \quad (14)$$

$$t = 0 \quad q_i = 0 \quad c_i = 0 \quad (15)$$

where L is the length of the fixed bed (cm). $c_{\text{in},i}$ is the solute concentration at the inlet (mol/L).

The calculation method of axial diffusivity is shown in the Supporting Information.

The solution method of the above model equations is the same as that of the modified liquid-film linear driving force model.

■ ASSOCIATED CONTENT

SI Supporting Information

The Supporting Information is available free of charge at <https://pubs.acs.org/doi/10.1021/acsomega.2c05194>.

Adsorption isotherms of L-Trp at different pH values and calculation method of axial diffusion coefficient (PDF)

■ AUTHOR INFORMATION

Corresponding Author

Pengfei Jiao – Research Center of Henan Provincial Agricultural Biomass Resource Engineering and Technology, College of Life Science and Agricultural Engineering, Nanyang Normal University, Nanyang 473061 Henan, China; orcid.org/0000-0001-6918-2162; Phone: +86-0377-63513605; Email: jiaopf126@126.com; Fax: +86-0377-63512517

Authors

Xin Zhang – Research Center of Henan Provincial Agricultural Biomass Resource Engineering and Technology, College of

Life Science and Agricultural Engineering, Nanyang Normal University, Nanyang 473061 Henan, China

Yuping Wei – Research Center of Henan Provincial Agricultural Biomass Resource Engineering and Technology, College of Life Science and Agricultural Engineering, Nanyang Normal University, Nanyang 473061 Henan, China; orcid.org/0000-0002-0069-3906

Peng Wang – Research Center of Henan Provincial Agricultural Biomass Resource Engineering and Technology, College of Life Science and Agricultural Engineering, Nanyang Normal University, Nanyang 473061 Henan, China

Complete contact information is available at:

<https://pubs.acs.org/10.1021/acsomega.2c05194>

Notes

The authors declare no competing financial interest.

■ ACKNOWLEDGMENTS

This work was supported by the Science and Technology Department of Henan Province (grant no. 202102110285) and Nanyang Normal University (grant no. 2018ZX009).

■ REFERENCES

- Halan, V.; Maity, S.; Bhambure, R.; Rathore, A. S. Multimodal Chromatography for Purification of Biotherapeutics – A Review. *Curr. Protein Pept. Sci.* **2017**, *20*, 4–13.
- Wang, X.; Peng, J.; Peng, H.; Chen, J.; Xian, X.; Ni, J.; Li, H.; Long, J.; Zhang, H.; Ni, R.; Li, S.; Long, D.; Zhang, Z. Preparation of two ionic liquid bonded stationary phases and comparative evaluation under mixed-mode of reversed phase/ hydrophilic interaction/ ion exchange chromatography. *J. Chromatogr. A* **2019**, *1605*, 460372–460381.
- Zuo, H.; Guo, Y.; Zhao, W.; Hu, K.; Wang, X.; He, L.; Zhang, S. Controlled Fabrication of Silica@Covalent Triazine Polymer Core-Shell Spheres as a Reversed-Phase/Hydrophilic Interaction Mixed-Mode Chromatographic Stationary Phase. *ACS Appl. Mater. Interfaces* **2019**, *11*, 46149–46156.
- Gao, J.; Luo, G.; Li, Z.; Li, H.; Zhao, H.; Qiu, H. A new strategy for the preparation of mixed-mode chromatographic stationary phases based on modified dialdehyde cellulose. *J. Chromatogr. A* **2020**, *1618*, 460885–460895.
- Wu, Q.; Lin, D.; Shi, W.; Zhang, Q.; Yao, S. A mixed-mode resin with tryptamine ligand for human serum albumin separation. *J. Chromatogr. A* **2016**, *1431*, 145–153.
- Shi, W.; Zhang, S.; Li, K.; Jia, W.; Han, H. Integration of mixed-mode chromatography and molecular imprinting technology for double recognition and selective separation of proteins. *Sep. Purif. Technol.* **2018**, *202*, 165–173.
- Li, M.; Zou, X.; Zhang, Q.; Lin, D.; Yao, S. Binding mechanism of functional moieties of a mixed-mode ligand in antibody purification. *Chem. Eng. J.* **2020**, *400*, 125887–125894.
- Bäurer, S.; Polnick, S.; Sánchez-Muñoz, O. L.; Kramer, M.; Lämmerhofer, M. N-Propyl-N'-2-pyridylurea-modified silica as mixed-mode stationary phase with moderate weak anion exchange capacity and pH-dependent surface charge reversal. *J. Chromatogr. A* **2018**, *1560*, 45–54.
- Kazarian, A. A.; Barnhart, W.; Long, J.; Sham, K.; Wu, B.; Murray, J. K. Purification of N-acetylgalactosamine-modified-oligonucleotides using orthogonal anion-exchange and mixed-mode chromatography approaches. *J. Chromatogr. A* **2022**, *1661*, 462679.
- Koppejan, V.; Ferreira, G.; Lin, D. Q.; Ottens, M. Mathematical modelling of expanded bed adsorption—a perspective on in silico process design. *J. Chem. Technol. Biotechnol.* **2018**, *93*, 1815–1826.
- Li, R.; Sun, W.; Xiao, X.; Chen, B.; Wei, Y. Retention of stevioside polar compounds on a sulfonic acid-functionalized cation

exchange stationary phase. *J. Chromatogr. A* **2020**, *1620*, 460978–460984.

(12) Obradović, D.; Komsta, U.; Agbaba, D. Novel computational approaches to retention modeling in dual hydrophilic interactions/reversed phase chromatography. *J. Chromatogr. A* **2020**, *1619*, 460951.

(13) Bi, J.; Wang, J.; Ferguson, S.; Huang, X.; Tao, H.; Li, G.; Wang, T.; Hao, H. Modeling of Mixed Mechanism Adsorption Processes Driven by Surface Adsorption and Internal Ion Exchange. *Ind. Eng. Chem. Res.* **2020**, *59*, 14467–14475.

(14) Dores-Sousa, J. L.; De Vos, J.; Kok, W. T.; Eeltink, S. Probing selectivity of mixed-mode reversed-phase/weak-anion-exchange liquid chromatography to advance method development. *J. Chromatogr. A* **2018**, *1570*, 75–81.

(15) Gomes, P. F.; Loureiro, J. M.; Rodrigues, A. E. Expanded bed adsorption of albumin and immunoglobulin G from human serum onto a cation exchanger mixed mode adsorbent. *Adsorption* **2018**, *24*, 293–307.

(16) Chester, T. L. The combination of partition, size exclusion, and hydrodynamic models in chromatography, and application to bonded phases on porous supports. *J. Chromatogr. A* **2020**, *1620*, 461011–461019.

(17) Jiao, P.; Wang, Z.; Zhang, C.; Ali, M.; Gu, L.; Gao, S.; Liu, J. Adsorption separation of guanosine 5'-Monophosphate and cytidine 5'-Monophosphate by mixed-mode Resin HD-1: Experimental study and mathematical modeling. *J. Chromatogr. A* **2022**, *1678*, 463359–463368.

(18) Pham, K. N.; Lewis-Ballester, A.; Yeh, S. R. Conformational Plasticity in Human Heme-Based Dioxygenases. *J. Am. Chem. Soc.* **2021**, *143*, 1836–1845.

(19) Xu, Q.; Bai, F.; Chen, N.; Bai, G. Utilization of acid hydrolysate of recovered bacterial cell as a novel organic nitrogen source for L-tryptophan fermentation. *Bioengineered* **2019**, *10*, 23–32.

(20) Minliang, C.; Chengwei, M.; Lin, C.; Zeng, A.-P. Integrated laboratory evolution and rational engineering of GalP/Glk-dependent *Escherichia coli* for higher yield and productivity of L-tryptophan biosynthesis. *Metab. Eng. Commun.* **2021**, *12*, No. e00167.

(21) Niu, H.; Li, R.; Liang, Q.; Qi, Q.; Li, Q.; Gu, P. Metabolic engineering for improving L-tryptophan production in *Escherichia coli*. *J. Ind. Microbiol. Biotechnol.* **2019**, *46*, 55–65.

(22) Xiong, B.; Zhu, Y.; Tian, D.; Jiang, S.; Fan, X.; Ma, Q.; Wu, H.; Xie, X. Flux redistribution of central carbon metabolism for efficient production of L-tryptophan in *Escherichia coli*. *Biotechnol. Bioeng.* **2021**, *118*, 1393–1404.

(23) Zhao, C.; Fang, H.; Wang, J.; Zhang, S.; Zhao, X.; Li, Z.; Lin, C.; Shen, Z.; Cheng, L. Application of fermentation process control to increase L-tryptophan production in *Escherichia coli*. *Biotechnol. Prog.* **2020**, *36*, No. e2944.

(24) Jiao, P.; Zhang, X.; Li, N.; Wei, Y.; Wang, P.; Yang, P. Cooperative adsorption of L-tryptophan and sodium ion on a hyper-cross-linked resin: Experimental studies and mathematical modeling. *J. Chromatogr. A* **2021**, *1648*, 462211–462219.

(25) Xie, Y.; Jing, K.; Lu, Y. Kinetics, equilibrium and thermodynamic studies of L-tryptophan adsorption using a cation exchange resin. *Chem. Eng. J.* **2011**, *171*, 1227–1233.

(26) Luo, W.; Wei, P.; Chen, H.; Fan, L.; Huang, L.; Huang, J.; Xu, Z.; Cen, P. Kinetics and optimization of L-tryptophan separation with ion-exchange chromatography. *Korean J. Chem. Eng.* **2011**, *28*, 1280–1285.

(27) Jiao, P.; Wei, Y.; Zhang, M.; Zhang, X.; Zhang, X.; Yuan, X. Adsorption separation of L-tryptophan based on the hyper-cross-linked resin XDA-200. *ACS Omega* **2021**, *6*, 2255–2263.

(28) Jiao, P.; Zhang, X.; Wei, Y.; Meng, Y. Adsorption equilibria, kinetics and column dynamics of L-tryptophan on mixed-mode resin HD-1. *ACS Omega* **2022**, *7*, 9614–9621.

(29) Keken-Huskey, P. M.; Gillette, A. K.; Mccammon, J. A. Predicting the influence of long-range molecular interactions on macroscopic-scale diffusion by homogenization of the Smoluchowski equation. *J. Chem. Phys.* **2015**, *140*, 174106–174112.

(30) Schmidt-Traub, H. *Preparative Chromatography of Fine Chemicals and Pharmaceutical Agents*; Wiley-Vch: Weinheim, 2005.